Polym. Bull. (2015) 72:1937–1948
DOI 10.1007/s00289-015-1381-9

ORIGINAL PAPER

Poly(ethylene oxide)/graphene oxide nanocomposites: structure, properties and shape memory behavior

Young-Wook Chang[1] · Kang-Suk Lee[1] · Yong-Woo Lee[2] · Jin Ho Bang[2]

Received: 16 October 2014 / Revised: 15 February 2015 / Accepted: 4 April 2015 /
Published online: 16 April 2015

Abstract Poly(ethylene oxide) (PEO)/graphene oxide (GO) nanocomposites with GO contents of 1, 3, 5 and 7 wt% were prepared by solution mixing followed by film casting. Field-emission scanning electron microscopy observations showed that the GO nanosheets are dispersed uniformly in the PEO matrix. Fourier transform infrared (FTIR) and X-ray photoelectron spectroscopy (XPS) analysis of the nanocomposites revealed that there are hydrogen-bonded interactions between surface carboxylic acid on the GO sheets and ether group of the PEO. Differential scanning calorimetry (DSC), tensile testing, and dynamic mechanical analysis (DMA) showed that, with increasing GO content in the nanocomposites, the melting temperature and degree of crystallinity decreased while glass transition temperature, tensile modulus, strength and elongation-at-break concurrently increased. DMA results also demonstrated the presence of a rubbery plateau above the melting temperature of the PEO/GO nanocomposites, and the moduli at the plateau region increased with increasing GO content in the nanocomposites, implying that the PEO/GO nanocomposites formed a physically crosslinked structure. PEO/GO nanocomposites with GO contents higher than 5 wt% exhibited excellent thermally and infrared-triggered shape memory behavior.

✉ Young-Wook Chang
ywchang@hanyang.ac.kr

[1] Department of Chemical Engineering, Polymer Nano Materials Laboratory, Hanyang University, Ansan, Kyunggi-Do, Korea

[2] Department of Chemistry and Applied Chemistry, Hanyang University, Ansan, Kyunggi-Do, Korea

Introduction

Recently, graphene oxide (GO) has emerged as a new promising nanofiller for polymers due to its unique structural, mechanical, thermal, and electro-optical properties [1–3]. The GO can be readily exfoliated into single-layered or few-layered sheets in aqueous or organic solvents. Functional groups that exist on GO surfaces can form strong interactions with host polymers. A variety of polymer/GO nanocomposites have been investigated over the past few years based on various polymer matrices such as polyurethane [4, 5], poly(ε-caprolactone) [6], ethylene vinyl acetate [7], Nafion [8], and some water soluble polymers including chitosan [9, 10], poly(vinyl alcohol) [11–14], poly(allyl amine) [15], and poly(acrylamide) [16].

Poly(ethylene oxide) (PEO) is an important semicrystalline polymer that can be used for biomedical and electrochemical applications [17–19]. The problem in these applications is the poor mechanical properties of PEO above its melting temperature. To improve the mechanical properties of PEO, nanocomposites with various nanofillers such as clay [20–22], cellulose nanowhiskers [23, 24], carbon nanotubes [25, 26] and silica nanoparticles [27] have been explored. Physically crosslinked structure was realized in the PEO nanocomposites with nanoparticles having strong interfacial interactions with matrix PEO, which provide thermal stabilization of storage modulus above the melting point of the nanocomposite [23, 24].

It is well known that crosslinked polymers containing crystalline PEO exhibit shape memory effects [28–30]. In the systems, crystalline domain of PEO serves as a reversible switching phase and crosslink points serve as fixed points, which enable the polymer to recover to its original shape after being deformed into a temporary shape when it is heated above its crystalline melting temperature. Various nanofillers can be incorporated into the shape memory polymers to enhance their mechanical properties and trigger the shape recovery by infrared light [31, 32], electric [33, 34] or magnetic field [35]. Such shape memory polymers have various potential applications such as in actuators, robotics, microelectromechanical systems, and biomedical devices.

The goal of the present work is to explore the reinforcing effects GO in PEO nanocomposites. We observed that storage modulus of the PEO/GO nanocomposites is stabilized above their melting temperature, which enabled the nanocomposite to exhibit shape memory behavior. Detailed thermomechanical properties of the PEO/GO nanocomposites are examined to support this.

Experimental

Materials

Poly(ethylene oxide) (PEO) (Mw = 600,000) was purchased from Aldrich. Graphene oxide (GO) was synthesized according to Hummers' method with some modification [36, 37]. Graphite powder (200 mg) was dispersed in sulfuric acid (9.2 mL) containing sodium nitrate (200 mg) and sonicated in an ice bath for

10 min. Potassium permanganate (1.2 g) was slowly added to the graphite suspension under sonication, taking care that the temperature of the suspension did not exceed ~20 °C. The suspension was then removed from the ice bath and heated at a temperature of 35–40 °C for 1 h. Deionized water was subsequently added to the reaction vessel very carefully under stirring to prevent overheating above 100 °C. The suspension was kept at 80–90 °C for an additional 20 min, and hydrogen peroxide (3 %, 60 mL) was added to the suspension. The resulting brown powder was collected by centrifugation and washed twice with hydrogen chloride (1 M) and deionized water to remove unreacted species. The GO powder was achieved after drying under vacuum at 60 °C for 24 h. The GO readily forms a stable colloidal suspension in aqueous medium after suitable ultrasonic treatment. Figure 1 shows the bright-field TEM images of the synthesized GOs. The TEM samples are prepared by placing a drop of diluted dispersion onto holey carbon grids. It can be seen that GO has a typical shape resembling the large crumpled thin flake [36].

Blend preparation

The PEO/GO hybrids with GO content of 1, 3, 5 and 7 wt% were prepared by mixing the PEO/water solution and GO aqueous dispersion by sonication at room temperature in an ultrasonic bath (KIG 2000SG, Kyung Il Ultrasonic Ltd., Korea) at an applied frequency of 40 kHz and power of 600 W. PEO was dissolved in water over 2 days. GO was dispersed in water with the aid of sonication for 1 h, and the desired amount of GO (water dispersion) was added gradually into aqueous PEO solution with constant stirring. The resulting mixture was sonicated for 3 h, which was performed intermittently with water circulation so that the bath temperature does not exceed 30 °C. The resulting mixture was poured into a Teflon Petri dish and was dried in a vacuum oven at room temperature for 10 days to remove the water. Films with a thickness of about 100 μm were ultimately obtained.

Characterization of PEO/GO hybrids

The phase morphology of the PEO/GO hybrid was observed by field-emission scanning electron microscopy (FE-SEM, JEOL JSM-630F) at an accelerating voltage of 15 kV. All of the samples were fractured after immersion in liquid

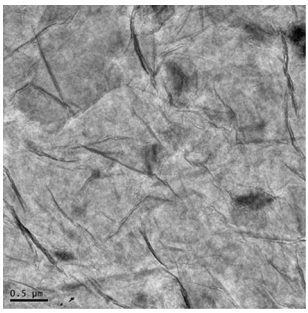

Fig. 1 TEM image of the synthesized GO

nitrogen for about 10 min. The fracture surface was then coated with a thin layer of gold.

FTIR analysis of the PEO/GO nanocomposite samples was conducted using an attenuated total reflectance on a Varian 800 Infrared Fourier Transform Spectrometer (Varian, Inc.).

X-ray photoelectron spectroscopy (XPS) spectra of neat PEO, neat GO and PEO/GO nanocomposites were recorded using an X-ray photoelectron spectrometer (K-Alpha, Thermo Fisher Scientific, Inc.) with aluminum (mono) Kα X-ray source (1486.6 eV) operated at a 15 kV voltage and 10 mA current. A high-resolution survey was performed for all samples at spectral regions related to carbon and silicon atoms.

Dynamic mechanical tests were performed using a dynamic mechanical analyzer (TA Instrument 2980). Samples were subjected to a cyclic tensile strain with an amplitude of 0.2 % at a frequency of 1 Hz. The temperature was increased at a heating rate of 10 °C/min over the range of −100 to 100 °C.

Tensile properties were measured using universal testing machine (Unites Co, STM 10 E) at 25 °C and a crosshead speed of 50 mm/min according to ASTM D 638.

The melting temperature (T_m), heat of fusion (ΔH_m) and non-isothermal crystallization temperature (T_c) of neat PEO and PEO/GO hybrids were determined using a differential scanning calorimeter (TA Instruments DSC 2010). Samples (10 mg) were dried completely in a vacuum oven and then used for analysis. They were first heated from 30 to 100 °C at a rate of 10 °C min^{-1} under a nitrogen atmosphere and were then held for 10 min at this temperature to remove prior thermal history. The samples were then cooled to −30 °C at a rate of 10 °C min^{-1}, and the crystallization peak temperature (T_c) was determined from the thermogram. Subsequently, the sample was reheated to 100 °C at a rate of 10 °C min^{-1} (second scan) to determine T_m and ΔH_m of the samples.

Shape memory behavior of the samples was investigated using dog-bone-shaped specimens with a thickness of about 100 μm (as shown in Fig. 8). The samples were deformed to 100 % of gage length at room temperature, and all the samples were found to be fixed well at the deformed shape. Then all the temporarily deformed samples were heated at 70 °C to analyze the shape recovery. The shape recovery was also tested upon irradiation of the samples with infrared light (intensity: 70 mW/cm^2). An infrared (IR) lamp with a red filter (Philips, Model Infraphil PAR38E, Germany) was used as the light source, which was positioned at 30 cm from the sample.

Results and discussion

Field-emission SEM micrograph of the cross-section of the PEO/GO composite is shown in Fig. 2. The micrographs demonstrate that GO nanosheets of 50–120 nm thickness were uniformly dispersed in the PEO matrix with a planar orientation when the GO content was as high as 7 wt%. The uniform and nanoscaled dispersion

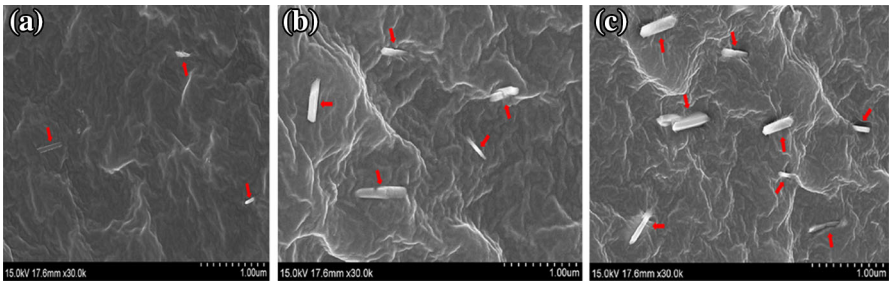

Fig. 2 FE-SEM micrographs of the cryogenically fracture surface of PEO/GO nanocomposites. **a** 97/3, **b** 95/5, and **c** 93/7

of GO implied that there were sufficient interactions between PEO matrix and GO sheets.

Interactions between the ether groups of PEO chains (C–O–C) and polar functional groups on the GO nanosheets such as COOH and –OH groups were examined by FTIR analysis, and the FTIR spectra are presented in Fig. 3. The IR peak of the neat PEO showed the C–O–C asymmetric stretch at 1106 cm^{-1}, and this peak shifted to a higher wavenumber for the PEO/GO nanocomposites with increased GO content. Similar results were observed in previously studied PEO/hydroxypropyl methylcellulose blend [38]. These results support that hydrogen bonds formed between the PEO and GO, which induced nanoscaled dispersion of GO in PEO matrix.

The XPS analysis was carried out to get further evidence for the formation of hydrogen bonds between GO and PEO. The XPS spectra for neat PEO and PEO/GO nanocomposites are shown in Fig. 4. The binding energy was reduced for the ether oxygen atom (O_{1s}) in PEO from 531.18 for neat PEO to 530.6 eV in the PEO/GO (93/7) nanocomposite. This reduction was attributed to the formation of hydrogen bonds between polar functional groups present on the GO surface and the ether oxygens of the PEO chain.

Figure 5a, b shows the variation of storage modulus and tan δ with temperature for neat PEO and PEO/GO nanocomposites, respectively, and the results are summarized in Table 1. As shown in Fig. 5a, the storage moduli for the nanocomposites are higher than those of the neat PEO over the whole temperature range examined, and the modulus increased with increasing GO content, implying that the GO nanoparticles acted as reinforcing fillers. As shown in Fig. 5a, the storage modulus for neat PEO continues to decrease with temperature, and the material flows like a viscous liquid when the temperature is greater than the T_m of the crystalline PEO domains, whereas the PEO/GO nanocomposites showed a persistent rubbery plateau above the T_m. And, the storage modulus values in the rubbery region increase with increasing GO content in the nanocomposites, as shown in Fig. 5a and Table 1. The presence of a persistent rubbery plateau in the PEO/GO nanocomposites indicates that the nanocomposites form a crosslinked structure. The formation of a crosslinked structure due to close interactions between polymer matrix and inorganic nanoparticles was also observed in other polymer/

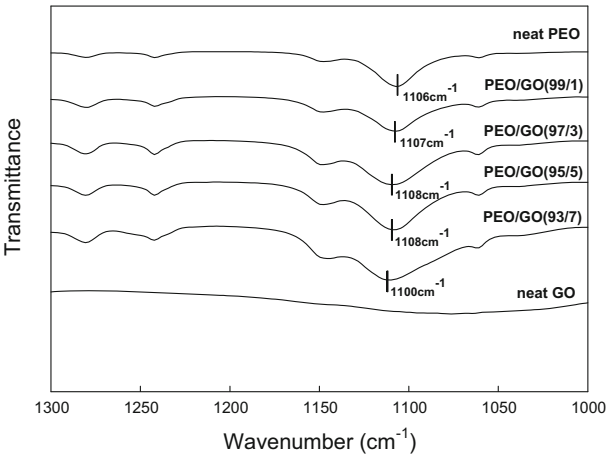

Fig. 3 FT-IR spectra of neat PEO, neat GO and PEO/GO nanocomposites

Fig. 4 XPS of O_{1s} of neat PEO and PEO/GO nanocomposites

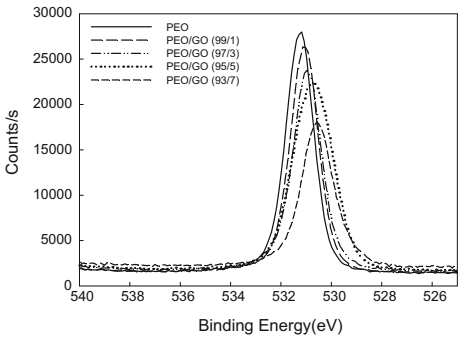

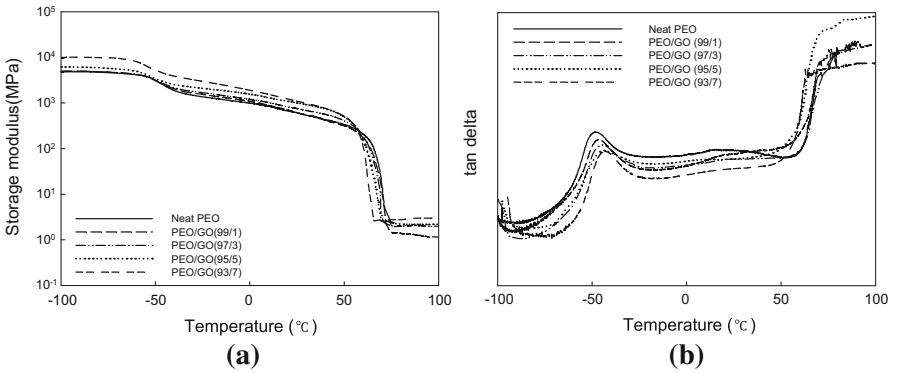

Fig. 5 Variations of **a** storage modulus and **b** tan δ with temperature of neat PEO and PEO/GO nanocomposites

Table 1 Dynamic mechanical properties of PEO/GO nanocomposites

Samples	T_g (°C)	E' at 30 °C (MPa)	E' at 80 °C (MPa)
Neat PEO	−47.9	538	0
PEO/GO			
99/1	−46.5	543	1.15
97/3	−44.6	679	2.00
95/5	−44.2	914	2.20
93/7	−43.1	978	2.95

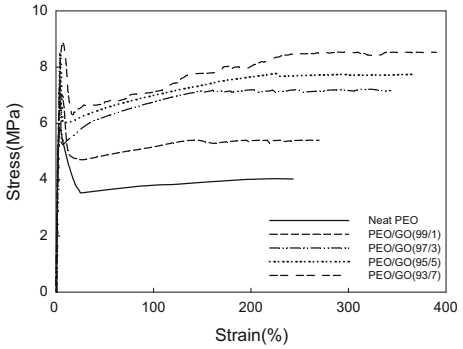

Fig. 6 Tensile stress–strain curves of neat PEO and PEO/GO nanocomposites

inorganic nanocomposites such as poly(vinyl alcohol)/GO nanocomposites [12], PEO/cellulose nanocomposite [23, 24], and poly(lactide)/hydroxyapatite nanocomposite [39].

It is evident from Fig. 5b that the position of the peak maximum in tan δ, which is related to the glass transition temperature (T_g), of the PEO/GO nanocomposites shifted toward a higher value compared to that of neat PEO. This indicates that the molecular mobility of amorphous PEO chains is constrained in the PEO/GO nanocomposites due to strong hydrogen-bonding interactions between PEO and GO.

Stress–strain curves of neat PEO and PEO/GO nanocomposites are shown in Fig. 6, and the results are summarized in Table 2. Neat PEO and PEO/GO nanocomposites exhibited similar stress–strain behaviors, and the nanocomposites showed higher tensile modulus and yield strength compared to neat PEO. It is interesting to note that both tensile strength and elongation-at-break increased concurrently in the nanocomposites, which has also been observed in other polymer/GO nanocomposites. This behavior can be explained in terms of slippage of polymer chains by finely dispersed GO nanosheets inducing stress concentrations under tensile stress. This process should enable the polymer molecules to release the tensile stress during extension, resulting in enhanced ductility [9, 16, 20].

Thermal characterization of the PEO/GO nanocomposites was carried out using DSC measurements, and the thermograms are shown in Fig. 7. The non-isothermal crystallization temperature (T_c), melting temperature (T_m), heat of fusion ($\triangle H_m$), and associated degree of crystallinity (χ_c) obtained from the DSC thermograms are

Table 2 Tensile properties of PEO/GO nanocomposites

Samples	E (MPa)	ε_y (%)	σ_y (MPa)	ε_b (%)	σ_b (MPa)
Neat PEO	165 ± 5	3.8 ± 0.1	5.1 ± 0.2	243 ± 2	4.0 ± 0.2
PEO/GO					
99/1	188 ± 6	3.9 ± 0.1	7.0 ± 0.2	270 ± 2	5.4 ± 0.2
97/3	212 ± 7	4.2 ± 0.1	7.5 ± 0.2	343 ± 3	7.2 ± 0.3
95/5	226 ± 7	4.2 ± 0.1	8.5 ± 0.3	364 ± 3	7.7 ± 0.3
93/7	296 ± 8	5.8 ± 0.2	8.9 ± 0.3	390 ± 3	8.5 ± 0.3

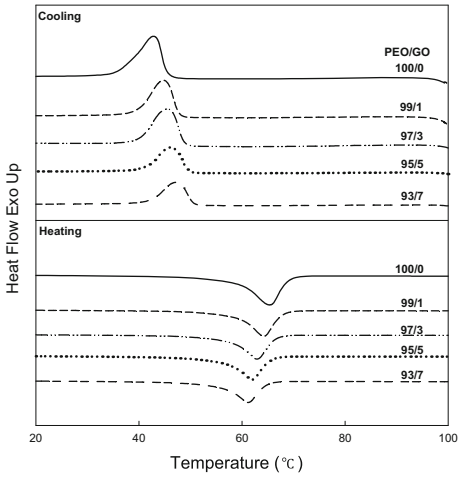

Fig. 7 DSC thermograms of neat PEO and PEO/GO nanocomposites

listed in Table 3. The degree of crystallinity of the nanocomposites was calculated using the heat of fusion per gram of PEO determined from DSC measurements and the heat of fusion corresponding to 100 % crystalline PEO (205 J/g) [23, 40].

As illustrated in the table, T_c, T_m and χ_c of the PEO/GO nanocomposites were decreased as the GO content increased. This trend is associated with the crosslinked nature of the nanocomposites, as discussed above. With increasing GO content, i.e., with increasing crosslink density, the molecular mobility of polymer chains decreased, restricting the crystallization of the polymer.

We observed thermally triggered shape memory behavior in the PEO/GO nanocomposites, as demonstrated in Fig. 8. When stretched to 100 % at room temperature, all nanocomposite samples underwent plastic deformation accompanied with yielding and their elongated shape was fixed immediately after the tensile load was removed. Upon heating the deformed samples at 70 °C (which is above the T_m of the samples), the PEO/GO nanocomposite samples shrank and recovered to their original shape within 30 s. Such thermally triggered shape memory effects can be seen in polyester–polyethylene glycol multiblock copolymers [28, 29] and chemically crosslinked polymer containing PEO [30]. These shape memory

Table 3 Thermal characteristics of PEO/GO nanocomposites

Samples	T_c (°C)	T_m (°C)	ΔH_m (J/g)	χ_c^a (%)
Neat PEO	42.8	65.3	132.6	64.7
PEO/GO				
99/1	44.8	64.2	124.8	61.5
97/3	45.5	62.9	117.5	59.1
95/5	46.2	61.9	105.8	54.3
93/7	46.9	61.2	99.4	52.1

[a] $\chi_c = 100 \times (\Delta H_m/\Delta H_m^o)/w$, where ΔH_m^o is the heat of melting for 100 % crystalline PEO (205 J/g) [23, 40] and w is the weight fraction of PEO in the nanocomposites

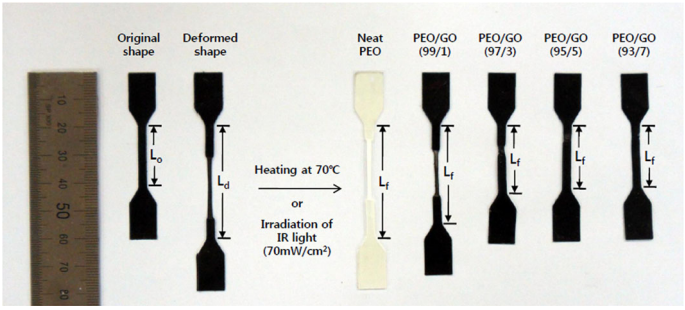

Fig. 8 Shape memory behavior of the samples

polymers consist of two separate phases, namely, stationary phase and reversible phase, where the crosslinked (chemically or physically) points stabilize the permanent shape and a second phase having a melting transition serves as a switch. In the PEO/GO nanocomposites, shape fixing occurred from the orientation of PEO chains toward the tensile deformation and formation of oriented crystals. And, the shape recovery could occur upon heating the temporary sample above the T_m of PEO, during which the PEO crystals are melted and the polymer chains obtain the activity to recover to its original shape with a release of the stored energy.

The final shape recovery ratio (R) of the samples was calculated by the following formula:

$$R = [(L_d - L_f)/(L_d - L_o)] \times 100\,(\%),$$

where L_o, L_d, and L_f are the original gage length, the deformed length, and the final recovery length of sample, respectively. The degree of recovery increased with increasing GO content in the nanocomposites, and the R value of the nanocomposite with a GO content of 1, 3. 5, and 7 wt% were 25, 89, 95, and 99 %, respectively. Improved shape recovery of the nanocomposites with higher GO content is ascribed to the formation of effective crosslinked points at higher GO nanoparticle content in the nanocomposites [12].

Figure 8 also demonstrated that the deformed PEO/GO nanocomposites recovered to their original shape when they are exposed to near IR irradiation. The nanocomposite sample with GO content of 5 wt% recovered to its original length with R value of 95 % within 1 min under the IR irradiation. This arises from excellent photothermal conversion efficiency and IR absorption ability of GO nanoparticles embedded in PEO matrix, which can directly transform photoenergy into thermal energy [3, 4, 32].

And, we observed that high shape retention and shape recovery can be maintained under repeated testing (confirmed up to five cycles). This indicates that the PEO/GO nanocomposites can retain stable shape memory effects under repeated use, which is of importance for practical applications.

Conclusions

PEO/GO nanocomposites, in which GO nanosheets are uniformly dispersed in PEO matrix, were prepared by a solvent-casting method. The FTIR and XPS results showed that hydrogen-bonding interactions between the PEO and the surface functional groups of GO exist in the PEO/GO nanocomposites. DSC, DMA, and tensile testing revealed that GO nanosheets act as physically crosslinked points and reinforcing fillers. PEO/GO nanocomposites with GO contents higher than 5 wt% exhibit excellent thermally and infrared-triggered shape memory behavior. Such novel shape memory PEO/GO nanocomposites may have many potential biomedical applications such as soft actuator, sensor, and micromechanical systems.

Acknowledgments This work was supported by a Grant (No. 405-111-004) funded by Ministry of Environment, Korea.

References

1. Zhu Y, Murali S, Cai W, Li X, Suk JW, Potts JR et al (2010) Graphene and graphene oxide: synthesis, properties, and applications. Adv Mater 22:3906–3924
2. Geim AK, Novoselov KS (2007) The rise of graphene. Nat Mater 6:183–191
3. Compton OC, Nguyen SBT (2010) Graphene oxide, highly reduced graphene oxide, and graphene: versatile building blocks for carbon-based materials. Small 6:711–723
4. Liang J, Xu Y, Huang Y, Zhang L, Wang Y, Ma Y, Li F, Guo T, Chen Y (2009) Infrared-triggered actuators from graphene-based nanocomposites. J Phys Chem 113:9921–9927
5. Yousefi N, Gudarzi MM, Zheng Q, Lin X, Shen X, Jia J, Sharif F, Kim JK (2013) Highly aligned, ultralarge-size reduced graphene oxide/polyurethane nanocomposites: mechanical properties and moisture permeability. Composites Part A Appl Sci Manfact 49:42–50
6. Zhang J, Qiu Z (2011) Morphology, crystallization behavior, and dynamic mechanical properties of biodegradable poly(ε-caprolactone)/thermally reduced graphene nanocomposites. Ind Eng Chem Res 50:13885–13891
7. Kuila T, Khanra P, Mishra AK, Kim NH, Lee JH (2012) Functionalized-graphene/ethylene vinyl acetate copolymer composites for improved mechanical and thermal properties. Polym Testing 31:282–289
8. Choi BG, Huh YS, Park YC, Jung DH, Hong WH, Park HS (2012) Enhanced transport properties in polymer electrolyte composite membranes with graphene oxide sheets. Carbon 50:5395–5402
9. Yang X, Tu Y, Li L, Shang S, Tao XM (2010) Well-dispersed chitosan/graphene oxide nanocomposites. Appl Mater Interf 2:1707–1713

10. Pan Y, Wu T, Bao H, Li L (2011) Green fabrication of chitosan films reinforced with parallel aligned graphene oxide. Carbohy Polym 83:1908–1915
11. Wang Y, Shi Z, Yu J, Chen L, Zhu J, Hu Z (2012) Tailoring the characteristics of graphite oxide nanosheets for the production of high-performance poly(vinyl alcohol) composites. Carbon 50:5525–5536
12. Qi X, Yao X, Deng S, Zhou T, Fu Q (2014) Water-induced shape memory effect of graphene oxide reinforced polyvinyl alcohol nanocomposites. J Mater Chem A 2:2240–2249
13. Morimune S, Nishino T, Goto T (2012) Poly(vinyl alcohol)/graphene oxide nanocomposites prepared by a simple eco-process. Polym J 44:1056–1063
14. Zhao X, Zhang Q, Chen D (2010) Enhanced mechanical properties of graphene-based poly(vinyl alcohol) composites. Macromolecules 43:2357–2363
15. Satti A, Larpent P, Gun'ko Y (2010) Improvement of mechanical properties of graphene oxide/poly(allylamine) composites by chemical crosslinking. Carbon 48:3376–3381
16. Liu R, Liang S, Tang XZ, Yan D, Li X, Yu ZZ (2012) Tough and highly stretchable graphene oxide/polyacrylamide nanocomposite hydrogels. J Mater Chem 22:14160–14167
17. Alcantar NA, Aydil ES, Israelachvili JN (2000) Polyethylene glycol-coated biocompatible surfaces. J Biomed Mater Res 51:343–351
18. Yang XQ, Hanson L, McBreen J, Okamoto Y (1995) Development of a new plasticizer for poly(-ethylene oxide)-based polymer electrolyte and the investigation of their ion-pair dissociation effect. J Power Sour 54:198–204
19. Mishra R, Rao KJ (1998) Electrical conductivity studies of poly(ethyleneoxide)-poly(vinylalcohol) blends. Solid State Ionics 106:113–127
20. Ratna D, Divekar S, Samui AB, Chakraborty BC, Banthia AK (2006) Poly(ethylene oxide)/clay nanocomposite: thermomechanical properties and morphology. Polymer 47:4068–4074
21. Abraham TN, Siengchin S, Ratna D, Karger-Kocsis J (2010) Effect of modified layered silicates on the confined crystalline morphology and thermomechanical properties of poly(ethylene oxide) nanocomposites. J Appl Polym Sci 118:1297–1305
22. Burgaz E (2011) Poly(ethylene-oxide)/clay/silica nanocomposites: morphology and thermomechanical properties. Polymer 52:5118–5126
23. Azizi Samir MAS, Alloin F, Sanchez JY, Dufresne A (2004) Cellulose nanocrystals reinforced poly(oxythyene). Polymer 45:4149–4157
24. Azizi Samir MAS, Chazeau L, Alloin F, Cavaille JY, Dufresne A, Sanchez JY (2005) POE-based nanocomposite polymer electrolytes reinforced with cellulose whiskers. Electrochmica Acta 50:3897–3903
25. Narh KA, Jallo L, Rhee KY (2008) The effect of carbon nanotube agglomeration on the thermal and mechanical properties of polyethylene oxide. Polym Comp 29:809–817
26. Abraham TN, Ratna D, Siengchin S, Karger-Kocsis J (2008) Rheological and thermal properties of poly(ethylene oxide)/multiwalled carbon nanotube composites. J Appl Polym Sci 110:2094–2101
27. Zhang Q, Archer LA (2002) Poly(ethylene oxide)/silica nanocomposites: structure and rheology. Langmuir 18:10435–10442
28. Wang M, Luo X, Ma D (1998) Dynamic mechanical behavior in the ethylene terephthalate-ethylene oxide copolymer with long soft segment as a shape memory material. Eur Polym J 34:1–5
29. Huang CL, Jiao L, Zhang JJ, Zeng JB, Yang KK, Wang YZ (2012) Poly(butylene succinate)-poly(ethylene glycol) multiblock copolymer: synthesis, structure, properties and shape memory performance. Polym Chem 3:800–808
30. Ratna D, Karger-Kocsis J (2011) Shape memory polymer system of semi-interpenetrating network structure composed of crosslinked poly(methyl methacrylate) and poly(ethylene oxide). Polymer 52:1063–1070
31. Zhang H, Xia H, Zhao Y (2012) Optically triggered and spatially controllable shape-memory polymer–gold nanoparticle composite materials. J Mater Chem 22:845–849
32. Kim JT, Kim BK, Kim EY, Park HC, Jeong HM (2014) Synthesis and shape memory performance of polyurethane/graphene nanocomposites. React Funct Polym 74:16–21
33. Lu H, Liang F, Gou J, Leng J, Du S (2014) Synergistic effect of Ag nanoparticle decorated graphene oxide and carbon fiber on electrical actuation of polymeric shape memory nanocomposites. Smart Mater Struct 23:085034
34. Lu H, Yao Y, Huang WM, Hui D (2014) Noncovalently functionalized carbon fiber by grafted self-assembled graphene oxide and the synergistic effect on polymeric shape memory nanocomposites. Compos B 67:290–295

35. Schmidt AM (2006) Electromagnetic activation of shape memory polymer networks containing magnetic nanoparticles. Macromol Rapid Commun 27:1168–1172
36. Stankovich S, Piner RD, Nguyen ST, Ruoff RS (2006) Synthesis and exfoliation of isocyanate-treated graphene oxide nanoplatelets. Carbon 44:3342–3347
37. Stankovich S, Piner RD, Chen XQ, Wu NQ, Nguyen ST, Ruoff RS (2006) Stable aqueous dispersions of graphitic nanoplatelets via the reduction of exfoliated graphite oxide in the presence of poly(sodium 4-styrenesulfonate). J Mater Chem 16:155–158
38. Fuller CS, MacRae RJ, Walther M, Cameron RE (2001) Interactions in poly(ethylene oxide)-hydroxypropyl methylcellulose blends. Polymer 42:9583–9592
39. Zhou S, Zheng X, Yu X, Wang J, Weng J, Li X et al (2007) Hydrogen bonding interaction of poly(D, L-lactide)/hydroxyapatite nanocomposites. Chem Mater 19:247–253
40. Vidotto G, Levy DL, Kovacs AJ (1969) Cristallisation et fusion des polymères autoensemencés. Kolloid Z Z Polym 230:289–305